Highly efficient CW laser operation in 4 at. % Tm^{3+} and 4 at. % Y^{3+} codoped CaF_2 crystals

Xinsheng Guo (郭新生)[1,2], Qinghui Wu (吴庆辉)[2], Linyang Guo (郭林炀)[3], Fengkai Ma (马凤凯)[2], Fei Tang (唐 飞)[2], Cheng Zhang (张 程)[4], Jie Liu (刘 杰)[4], Bingchu Mei (梅炳初)[1,*], and Liangbi Su (苏良碧)[2,5,]**

[1]*State Key Laboratory of Advanced Technology for Materials Synthesis and Processing, School of Materials Science and Engineering, Wuhan Institute of Technology, Wuhan 430070, China*

[2]*Synthetic Single Crystal Research Center, Key Laboratory of Transparent and Opto-Functional Inorganic Materials, Shanghai Institute of Ceramics, Chinese Academy of Sciences, Shanghai 201899, China*

[3]*State Key Laboratory on High Power Semiconductor Lasers, Changchun University of Science and Technology, Changchun 130022, China*

[4]*Shandong Provincial Key Laboratory of Optics and Photonic Device, College of Physics and Electronics, Shandong Normal University, Jinan 250014, China*

[5]*State Key Laboratory of High Performance Ceramics and Superfine Microstructure, Shanghai Institute of Ceramics, Chinese Academy of Sciences, Shanghai 201899, China*

**Corresponding author: bcmei@whut.edu.cn; **corresponding author: suliangbi@mail.sic.ac.cn*

Received February 9, 2018; accepted March 1, 2018; posted online April 25, 2018

Tm:CaF_2 and Tm,Y:CaF_2 single crystals were prepared by the temperature gradient technique. The spectral properties of Tm,Y:CaF_2 single crystals were investigated and compared with those of Tm:CaF_2. It was demonstrated that codoping with Y^{3+} ions could efficiently improve the spectroscopic properties. Tm,Y:CaF_2 crystals have larger absorption cross-sections at the pumping wavelength, larger mid-infrared stimulated emission cross-sections, and much longer fluorescence lifetimes of the upper laser level (Tm^{3+}:$^3H_4$ level) than Tm:CaF_2 crystals. Continuous-wave (CW) lasers around 1.97 μm were demonstrated in 4.0 at. % Tm,4.0 at. % Y:CaF_2 single crystals under 792 nm laser diode (LD) pumping. The best laser performance has been demonstrated with a low threshold of 0.368 W, a high slope efficiency of 54.8%, and a maximum output power of 1.013 W.

OCIS codes: 140.2020, 140.3070, 140.3380, 140.3480.
doi: 10.3788/COL201816.051401.

Tm^{3+}-ion-based laser materials operating at around 2.0 μm are being developed at an increasing pace in recent years[1–5]. Lasers around this specifc region have several atmospheric transparency windows and are strongly absorbed by water and biological tissues. The unique features of the mid-infrared (IR) domain make it very attractive for many applications, such as coherent laser radar[6], remote sensing[7], laser ablation of varicose veins *in vitro*[8], and medical surgery[9–11]. Moreover, lasers around 2 μm are suitable pumping sources for IR optical parametric oscillation (OPO)[12,13], which have wide applications in scientifc research, atmospheric pollution monitoring, and directional-IR countermeasure.

CaF_2 has been proved to be an excellent optical material with broad-band transparency and low phonon energy[14]. Trivalent rare-earth-ion-doped CaF_2 (RE^{3+}:CaF_2) crystals have very broad and smooth absorption and emission spectra due to heterovalent substitution of Ca^{2+} and different forms of charge compensation. Such broad spectra are suitable for femtosecond pulses. In Nd, Y:CaF_2 crystal, Qin *et al.* have achieved 103 fs using a diode pumping passively mode-locked technique[15]. In addition, pure CaF_2 is characterized by a high thermal conductivity of 9.7 $W \cdot mK^{-1}$ and is thus comparable to that found in the case of $Y_3Al_5O_{12}$ (YAG). Even though the thermal conductivity of the CaF_2-doped rare-earth ions is reduced[16], it is still higher than that of glass. Many studies have been conducted based on rare–earth-doped CaF_2 crystals, including Yb:CaF_2, Er:CaF_2, and Nd:CaF_2[17–21]. However, fewer studies have been performed using Tm:CaF_2 crystals in the 2 μm wavelength band, since 1.9 μm lasers based on the Tm:CaF_2 ceramics upon LD pumping have been demonstrated for the first time[22], to the best of our knowledge. So far, the laser of Tm:CaF_2 ceramic with 4% doping only emitted an output power of 60 mW with a slope efficiency of 5.5%[23]. The laser performance of the Tm:CaF_2 crystal with 1.34% doping has been reported with a slope efficiency of 41.0%[24]. Recently, a continuous-wave (CW) output power of 453 mW with a slope efficiency of 21% from a Tm,Y:CaF_2 laser was obtained[25], proving that the Tm,Y:CaF_2 crystal was a significant potential lasing material. However, the superiorities of Tm,Y:CaF_2 crystal compared with Tm:CaF_2 crystal were not been analyzed systematically.

In this Letter, comparative studies on spectroscopic properties between Tm:CaF_2 and Tm,Y:CaF_2 were performed for the first time, to the best of our knowledge.

As we know, the quenching effect will occur due to defects and impurities introduced by increasing concentration of rare-earth ions. We found that codoping of Y^{3+} ions in Tm:CaF_2 can alleviate the cluster quenching effect and improve the spectral performance. 4 at. % Tm,4 at. % Y:CaF_2 demonstrated the laser performance with a high slope efficiency of 54.8% and a maximum output power of 1.013 W. To the best of our knowledge, this is the highest slope efficiency and largest power reported in Tm^{3+}-doped CaF_2 crystals.

Tm:CaF_2 and Tm,Y:CaF_2 crystals were grown by the temperature gradient technique (TGT). The raw materials of grown crystals are CaF_2, TmF_3, and YF_3. To prevent oxidation in the growing process, 1 wt. % PbF_2 was added to the starting materials. All of the raw materials used for our experiment were of 99.99% purity. The weighed chemical powders were mixed thoroughly and then sealed in the graphite crucibles during the process of growth. The crystal samples were cut and then polished into a size of 10 mm × 10 mm × 2 mm for spectral measurements.

The room temperature absorption spectra were measured using a Jasco V-570 UV/visible (VIS)/near-IR (NIR) spectrophotometer. Fluorescence spectra were obtained using an FLS 980 time-resolved fluorimeter with grating blazed at 1820 nm and detected using a Hamamatsu InSb. Fluorescence decay curves measured at 1820 nm were obtained with FLS 980 spectrophotometers under an 808 nm pulse laser excitation with the frequency of 9 Hz and duration of 10 μs. All of the measurements were carried out at room temperature.

Figure 1 shows the X-ray diffraction (XRD) patterns of 4% Tm:CaF_2 and 4% Tm,4% Y:CaF_2 crystals compared with the standard pattern of the pure CaF_2 phase. No impurity peaks are found, and all of the diffraction peaks of the Tm:CaF_2 and Tm,Y:CaF_2 crystals are in good agreement with those of the pure CaF_2 phase. These suggested that Tm^{3+} and Y^{3+} ions have substitutionally entered the Ca^{2+} sites and the doping ions do not change the perovskite-like structure of the pure CaF_2 crystal. The structural parameters of these crystals were obtained by fitting the XRD data using the software JADE 6.0. The lattice parameters of 4% Tm,4% Y:CaF_2 crystal is a bit larger than those of 4% Tm:CaF_2 crystal. It is well in agreement with the fact that the radius of Y^{3+} is greater than that of Tm^{3+}.

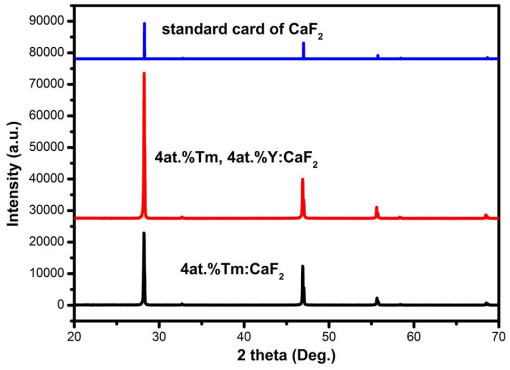

Fig. 1. XRD patterns of the Tm:CaF_2 and Tm,Y:CaF_2 crystals.

Figure 2 shows the room temperature absorption spectra of 4% Tm:CaF_2 and 4% Tm,4% Y:CaF_2 crystals in the wavelength range of 720–880 nm. There are three strong absorption peaks centered at 767, 784, and 792 nm, corresponding to the transitions from the ground state to the higher levels of Tm^{3+}.

The absorption coefficient and absorption cross-section at the strongest absorption peak of 767 nm in 4% Tm,4% Y:CaF_2 crystal are enhanced from 2.85 cm^{-1} and 0.34 × 10^{-21} cm^2 to 4.54 cm^{-1} and 4.7 × 10^{-21} cm^2, respectively, compared with 4% Tm:CaF_2 crystal. The larger absorption cross-section means a higher pump absorbing efficiency. The increasing of the absorption cross-section benefits from the stronger crystal field induced by codoping of Y^{3+} ions. While the crystallographic Ca^{2+} sites were occupied by the Y^{3+} ions, the compensation ions F^- were introduced to fill the vacancies of cubic lattices. This leads to distorted crystallographic sites and a stronger crystal field around Tm^{3+}.

According to the known absorption cross-section based on the reciprocity method, the emission cross-sections were calculated and shown in Fig. 3:

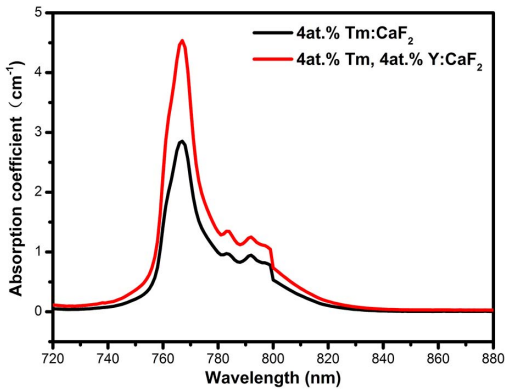

Fig. 2. Absorption spectra of Tm:CaF_2 and Tm,Y:CaF_2 crytals.

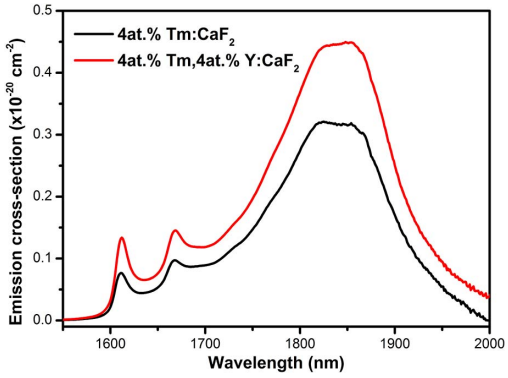

Fig. 3. Emission spectra of the Tm:CaF_2 and Tm,Y:CaF_2 crystals.

$$\sigma_{\mathrm{em}}(\lambda) = \sigma_{\mathrm{abs}}(\lambda)\frac{Z_L}{Z_u}\exp\left(\frac{E_{ZL} - hc/\lambda}{kT}\right), \quad (1)$$

where Z_u and Z_L are the partition functions of the lower and upper levels, E_{ZL} is the zero line energy defined as the energy gap between $^3H_6$ and $^3F_4$ manifolds, h is Planck's constant, k is Boltzmann's constant, and T is temperature. Here, the zero line is 1666 nm, and Z_u/Z_L is 1.512[11]. There are three emission peaks located at 1611, 1666, and 1820 nm, respectively. The emission cross-section of 4% Tm,4% Y:CaF_2 crystal was calculated to be 0.45×10^{-20} cm^2 at 1820 nm, which is increased by 40.96% compared with the value of 0.32×10^{-20} cm^2 in 4% Tm:CaF_2 crystal. The emission cross-section is enhanced by the incorporation of 4% Y^{3+} ions. There are two reasons to be concerned for the phenomenon. On the one hand, part of the f-f forbidden transition between $^3F_4$ and $^3H_6$ energy levels of Tm^{3+} ions was relieved by a stronger crystal field, as discussed above for absorption cross-sections. That is to say, higher absorption intensity results in a stronger emission in Tm,Y:CaF_2 crystal. On the other hand, it was pointed out that the Y^{3+} ions enter the lattice predominantly in the vicinity of the Tm^{3+} ions[26]. Thus, codoped Y^{3+} ions may separate the clustered Tm^{3+} ions in the lattice at an appropriate distance. As a result, the probability of cross-relaxation between Tm^{3+} ions was increased, and there will be more population inversion on the upper energy level. The emission was improved accordingly. Table 1 shows the comparison of the emission cross-section between our work and the Tm laser in other oxide hosts reported. The value of the Tm,Y:CaF_2 crystal is lower than those of YAG, $YAlO_3$ (YAP), and $C_{22}H_{36}NNaO_7S$ (SSO) but higher than that of $CaYAlO_4$. The data indicate that laser energy conversion efficiency of Tm:SSO is lower than those of YAP and CaF_2. In addition, the full widths at half-maximum of the emission peaks at 1820 nm of these samples were similar, which were about 200 nm.

The fluorescence decay curves of these samples excited by 808 nm pulsed lasers show a single exponential decay behavior, which are shown in Fig. 4. By fitting the decay curves, the lifetimes are obtained to be 2.99 and 3.94 ms in 4% Tm:CaF_2 crytal and 4% Tm,4% Y:CaF_2 crytal, respectively. The longer lifetime in Tm,Y:CaF_2 crystal further

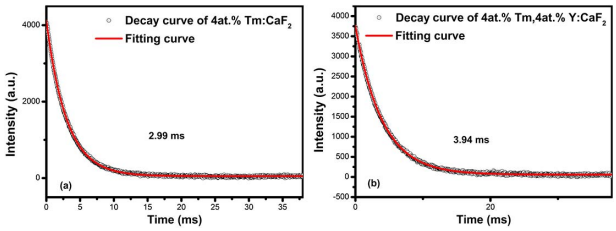

Fig. 4. Fluorescence decay curves at (a) 4 at. % Tm:CaF_2 and (b) 4 at. % Tm,4 at. % Y:CaF_2.

proved that codoping Y^{3+} is beneficial to luminescence. Moreover, compared to other oxide-based laser materials, the lifetime of Tm,Y:CaF_2 crystal is relatively long, which is listed in Table 1. Also, longer lifetime also means higher quantum efficiency.

As the absorption and emission cross-section were calculated, the gain cross-section σ_g could be estimated by the following equation:

$$\sigma_g = P \cdot \sigma_{\mathrm{abs}} - (1 - P) \cdot \sigma_{\mathrm{em}}, \quad (2)$$

where parameter P is the relative inverted population of the involved levels. The gain cross-sections of 4 at. % Tm:CaF_2 and 4 at. % Tm,4 at. % Y:CaF_2 crystals with the P varying from 0 to 0.4 were estimated and illustrated in Fig. 5. Obviously, the gain cross-section becomes positive when the population inversion level reaches 10%. In particular, the value of Tm,Y:CaF_2 is almost two times higher than that of Tm:CaF_2 crystal when the value of P is equal to 0.4.

CW laser operations were carried out by inserting an uncoated Tm,Y:CaF_2 sample inside a plane–concave laser resonator with water cooling at 13°C, and the setup was shown in Fig. 6. The pump source was a fiber-coupled 792 nm diode laser, delivering a maximum power of 30 W with a core diameter of 105 μm and a numerical aperture of 0.22. The pump beam was expanded into the gain medium by a coupling system of 1:2. M1 was a flat mirror (more than 90% transmission at the pump wavelength and more than 99% reflectivity at the lasing wavelength); M2 was a concave mirror having a radius of 100 mm with output transmissions of 2%, 5%, and 10% around 2.0 μm,

Table 1. Emission Cross-section, Emission Lifetime, and Laser Parameters of Tm-doped Hosts

Hosts	Emission Cross-section (cm^{-2})	Emission Lifetime (ms)	P_{out} (W)	η (%)	References
Tm:YAG	2.9×10^{-20}	0.25	0.593	18.9	[27]
Tm:SSO	6×10^{-21}	1.1	0.934	25.9	[28,29]
Tm:$CaYAlO_4$	2.5×10^{-21}	2.68–2.9	0.24	28	[30,31]
Tm:YAP	2.09×10^{-19}	48.3	10.5	46	[32,33]
Tm:CaF_2	3.2×10^{-21}	2.99	–	–	This work
Tm,Y:CaF_2	4.5×10^{-21}	3.94	1.013	54.8	This work

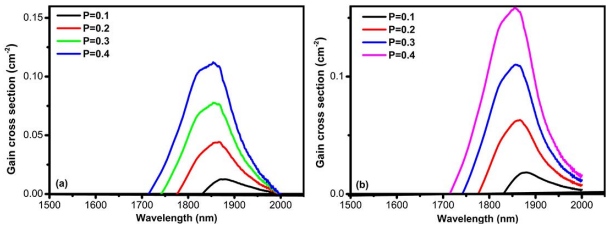

Fig. 5. Gain cross-section at (a) 4 at. % Tm:CaF_2 and (b) 4 at. % Tm,4 at. % Y:CaF_2.

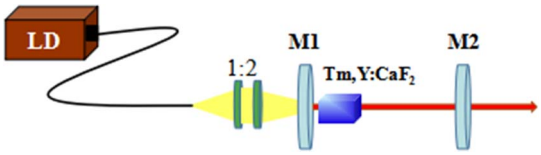

Fig. 6. Schematic of the Tm,Y:CaF_2 crystal laser.

respectively. The cavity length was about 90 mm. The laser sample was in dimensions of 3 mm × 3 mm × 7 mm. Laser operations were demonstrated around 1.97 μm with an LD pumping at 792 nm.

As shown in Fig. 7, CW laser operations around 1.97 μm were demonstrated in 4 at. % Tm,4 at. % Y:CaF_2. A slope efficiency of 54.8% and a maximum output power of 1.013 W were achieved by using the 5% transmissive output coupler (OC). To the best of our knowledge, this is the highest slope efficiency and largest power reported in Tm^{3+}-doped CaF_2 crystals. A comparative study for laser properties of Tm,Y:CaF_2 with other oxide hosts is shown in Table 1. The η value of Tm,Y:CaF_2 crystal is 54.8%, which is the highest in these hosts. The data indicate that the laser energy conversion efficiency of Tm,Y:CaF_2 is lower than those of oxide materials. The laser output power is 1.013 W, which is remarkable. The laser slope efficiencies are 49.9% and 53.6% by using the OCs with transmissions of 2% and 10%, respectively. The maximum output powers are 0.976 and 0.867 W, respectively. In order to protect the crystal, the experiments were done at low incident pump powers. Therefore, higher output power can be achieved with the increasing pump power.

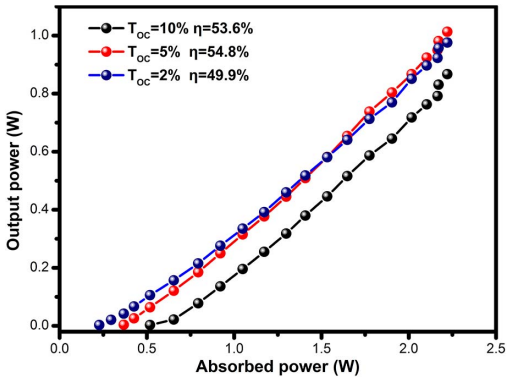

Fig. 7. Output powers versus absorbed pump power with output coupler transmissions of 2%, 5%, and 10%, respectively.

In summary, CaF_2 crystals doped with Tm^{3+} ions and Y^{3+} ions are obtained by the TGT. The fluorescent emissions around 1820 nm, corresponding to $^3F_4 \rightarrow {}^3H_6$ transitions of Tm^{3+}, were observed under the excitation of an 808 nm LD. The emission intensity at 1820 nm increased with codoping of Y^{3+} ions. Under LD pumping, a maximum CW output power of 1.013 W and a slop efficiency of 54.8% were obtained in the 4% Tm,4% Y:CaF_2 crystal. Further studies will foucus on Y^{3+} doping concentration in Tm:CaF_2 for potential CW lasers.

This work was financially supported by the National Natural Science Foundation of China (Nos. 61422511, 61635012, and 51432007) and the Strategic Priority Program of the Chinese Academy of Sciences (No. XDB16030000).

References

1. K. S. Lai, P. B. Phua, R. F. Wu, Y. L. Lim, E. Lau, S. W. Toh, B. T. Toh, and A. Chng, Opt. Lett. **25**, 1591 (2000).
2. P. Koopmann, S. Lamrini, K. Scholle, P. Fuhrberg, K. Petermann, and G. Huber, Opt. Lett. **36**, 948 (2011).
3. X. M. Duan, B. Q. Yao, Y. J. Zhang, C. W. Song, Y. L. Ju, and Y. Z. Wang, Chin. Opt. Lett. **6**, 591 (2008).
4. W. Liu, Y. L. Ju, T. Y. Dai, L. W. Xu, J. H. Yuan, C. Yang, B. Q. Yao, and X. M. Duan, Chin. Opt. Lett. **14**, 091401 (2016).
5. P. W. Kuan, X. K. Fan, W. T. Li, X. Q. Liu, C. L. Yu, L. Zhang, and L. L. Hu, Chin. Opt. Lett. **14**, 081601 (2016).
6. R. Targ, B. C. Steakley, J. G. Hawley, L. L. Ames, P. Forney, D. Swanson, R. Stone, R. G. Otto, and V. Zarifis, Appl. Opt. **35**, 7117 (1996).
7. U. N. Singh and J. R. Yu, in *Proc. IEEE Int. Conf. on Recent Advances in Space Technologies* (2003), p. 485.
8. A. N. Belyaev, A. N. Chabushkin, and S. A. Khrushchalina, Laser. Med. Sci. **31**, 503 (2016).
9. S. Wenk, S. Furst, V. Danicke, and D. T. Kunde, in *Advances in Medical Engineering*, T. M. Buzug ed. (Springer, 2007), p. 447.
10. B. Ropoulos, Photon. Spectra. **30**, 116 (1996).
11. J. G. Manni, Opt. Photon. News. **7**(7), 23 (1996).
12. P. A. Budni, L. A. Pomeranz, M. L. Lemons, C. A. Miller, J. R. Mosto, and E. P. Chicklis, J. Opt. Soc. Am. B. **17**, 723 (2000).
13. D. Creeden, P. A. Ketteridge, P. A. Budni, S. D. Setzler, Y. E. Young, J. C. McCarthy, and M. Jiang, Opt. Lett. **33**, 315 (2008).
14. A. A. Kaminskii, Laser. Photon. Rev. **1**, 93 (2010).
15. Z. P. Qin, G. Q. Xie, J. Ma, W. Y. Ge, P. Yuan, L. J. Qian, L. B. Su, D. P. Jiang, F. K. Ma, Q. Zhang, Y. X. Cao, and J. Xu, Opt. Lett. **39**, 1737 (2014).
16. P. A. Popov, P. P. Fedorov, V. M. Reiterov, E. A. Garibin, A. A. Demidenko, I. A. Mironov, and V. V. Osiko, Doklady Phys. **53**, 198 (2008).
17. M. Siebold, M. Hornung, R. Boedefeld, S. Podleska, S. Klingebiel, C. Wandt, F. Krausz, S. Karsch, R. Uecker, A. Jochmann, J. Hein, and M. C. Kaluza, Opt. Lett. **33**, 2770 (2008).
18. A. Kessler, M. Hornung, S. Keppler, F. Schorcht, M. Hellwing, H. Liebetrau, J. Körner, A. Sävert, M. Siebold, M. Schnepp, J. Hein, and M. C. Kaluza, Opt. Lett. **39**, 1333 (2014).
19. Z. P. Qin, G. Q. Xie, J. Ma, W. Y. Ge, P. Yuan, L. J. Qian, L. B. Su, D. P. Jiang, F. K. Ma, Q. Zhang, Y. X. Cao, and J. Xu, Opt. Lett. **39**, 1737 (2014).

20. F. K. Ma, D. P. Jiang, L. B. Su, J. Y. Wang, W. Cai, J. Liu, J. G. Zheng, W. G. Zheng, J. Xu, and Y. Liu, Opt. Lett. **41**, 501 (2016).
21. L. B. Su, Q. G. Wang, H. J. Li, G. Brasse, P. Camy, J. L. Doualan, A. Braud, R. Moncorgé, Y. Y. Zhan, L. H. Zheng, X. B. Qian, and J. Xu, Laser Phys. Lett. **10**, 035804 (2013).
22. P. A. Ryabochkina, Quantum Electron. **42**, 853 (2012).
23. A. A. Lyapin, P. P. Fedorov, E. A. Garibin, A. V. Malov, V. V. Osiko, P. A. Ryabochkina, and S. N. Ushakov, Opt. Mater. **35**, 1859 (2013).
24. P. Camy, J. L. Doualan, S. Renard, A. Braud, V. Menard, and R. Moncorge, Opt. Commun. **236**, 395 (2004).
25. X. Liu, K. Yang, S. Zhao, T. Li, C. Luan, X. Guo, B. Zhao, L. Zheng, L. Su, J. Xu, and J. Bian, Opt. Lett. **42**, 2567 (2017).
26. J. L. Doualan, P. Camy, R. Moncorgé, E. Daran, M. Couchaud, and B. Ferrand, J. Fluorine. Chem. **128**, 459 (2007).
27. B. J. Fei, J. Q. Huang, W. Guo, Q. F. Huang, J. Chen, F. Tang, W. C. Wang, and Y. G. Cao, J. Lumin. **142**, 189 (2013).
28. K. J. Yang, T. L. Feng, S. Z. Zhao, C. Liu, T. Li, W. W. Ma, Z. T. Zou, Q. G. Wang, L. B. Su, P. Solarz, R. Lisiecki, J. Komar, J. Xu, L. H. Zheng, and W. Ryba-Romanowski, J. Alloy. Compd. **712**, 412 (2017).
29. B. Liu, L. H. Zheng, Q. G. Wang, J. F. Liu, L. B. Su, H. L. Tang, J. Liu, X. W. Fan, F. Wu, P. Luo, H. Y. Zhao, J. J. Shi, N. T. He, N. Li, Q. Li, C. Guo, X. D. Xu, Z. S. Wang, and J. Xu, Chin. Phys. B **26**, 084203 (2017).
30. R. Moncorgk, N. Garnier, P. Kerbrat, C. Wyon, and C. Bore, Opt. Commun. **141**, 29 (1997).
31. Z. P. Qin, J. G. Liu, G. Q. Xie, J. Ma, W. L. Gao, L. J. Qian, P. Yuan, X. D. Xu, J. Xu, and D. H. Zhou, Laser Phys. **23**, 105806 (2013).
32. Y. L. Lu, Y. B. Dai, J. Wang, Y. Yang, A. P. Dong, S. H. Li, and B. D. Sun, Opt. Commun. **273**, 182 (2007).
33. C. Brian and G. Lew, Opt. Lett. **42**, 2259 (2000).